Oceanologia, uncorrected, in press
Polish Academy of Sciences
Institute of Oceanology
Open access article under the CC BY license
https://doi.org/10.5697/...

Trapped Contaminants in the Coastal Waters of the Southern Caspian Sea: off the Sefidrud River

Jafar Azizpour*, Reza Rahnama, Ali Hamzepoor, Seyed Masoud Mahmoudof

Abstract

Identifying and collecting accumulated contaminants is crucial for environmental protection in enclosed bodies of water, such as the Caspian Sea. As the world's largest landlocked water body, its limited exchange with open seas and oceans hinders self-purification. This research maps contaminant accumulation at the mouth of the Sefidrud River on the southern coast of the Caspian Sea using vessel-mounted ADCP, CTD, and water sampling data. Field measurements were conducted in two distinct seasons at different stations and transects ranging from 2–15 m in depth. The results show that the contaminants accumulated in the core of sub-mesoscale eddies. These surface sub-mesoscale eddies trap nutrient-rich freshwater discharging from the river, creating distinct hydrographic cores with significantly elevated nutrient levels, as well as different temperature and salinity compared to the surrounding waters.

Keywords
Caspian Sea; Sub-mesoscale eddy; Contaminants; Nutrients; Field measurements

[1] *Iranian National for Oceanography and Atmospheric Science, No. 3, Etemadzadeh St., Fatemi Ave., Tehran 1411813389, Iran*
***Correspondence**: azizpour@inio.ac.ir (J. Azizpour)

Received: 11 August 2024; **revised:** 1 December 2025; **accepted**: 8 December 2025

1. Introduction

The Caspian Sea (CS) is the world's largest landlocked water body, which extends >1000 km meridionally and contains more than 40% of the inland waters of the world. It is located in a depression separating Europe and Asia between the latitudes of 47°13' and 36°34'N and longitudes of 46°38' and 54°44'E (Azizpour and Ghaffari, 2023; Ehteshami et al., 2017; Safaian et al., 2004; Saleh et al., 2018)

More than 130 rivers flow into the CS, and the total river inflow is estimated to be around 300 km^3/yr. The contribution of the northern coast rivers is about 88% of the total river inflow, while the inflow along the western coast rivers accounts for 8% of the total inflow. The remaining inflow occurs along the Iranian coast. There is no permanent river inflow from the eastern coast (Ghaffari et al., 2010; Roshan et al., 2012; UNEP, 2006).

Industrial development and irregularly increasing population in rural and urban areas, followed by expansion of agricultural areas and fertilizer use, as well as excavation and exploitation of oil, have led to high amounts of industrial and homemade wastewater and agricultural runoff into the Caspian ecosystems. The pollution directly declines the Caspian biodiversity (Safaian et al., 2004).

The concentrations of pollutants, such as oil hydrocarbons, phenols, synthetic surfactants, organic matter, and metals, in river mouths frequently exceed maximum allowable concentrations by an order of 10 times or more and remain persistently high throughout the year. These pollutants generally originate from anthropogenic activities such as agriculture, mining, oil refining, industries, energy production, and shipping (CEP, 1998).

As an endorheic basin, the CS faces a fundamental challenge in self-purification owing to its disconnection from the open oceans. This isolation causes pollutants to persist and accumulate within the basin, as there is no outlet for their removal. Therefore, a precise understanding of contaminant inputs is critical for enabling early detection and facilitating effective, cost-efficient mitigation. Riverine discharges represent a major source of these contaminants, with the primary contributions stemming from agricultural, industrial, and urban activities (Aladin and Plotnikov, 2004; CEP, 2011).

Industrial pollution is increasing and exerting greater environmental pressure relative to other pollutant sources (Zaker et al., 2011). This issue is particularly acute along the southern coast, where a growing number of pollutant sources and a paucity of nearshore oceanographic data (Ghaffari and Chegini, 2010) create a critical knowl-

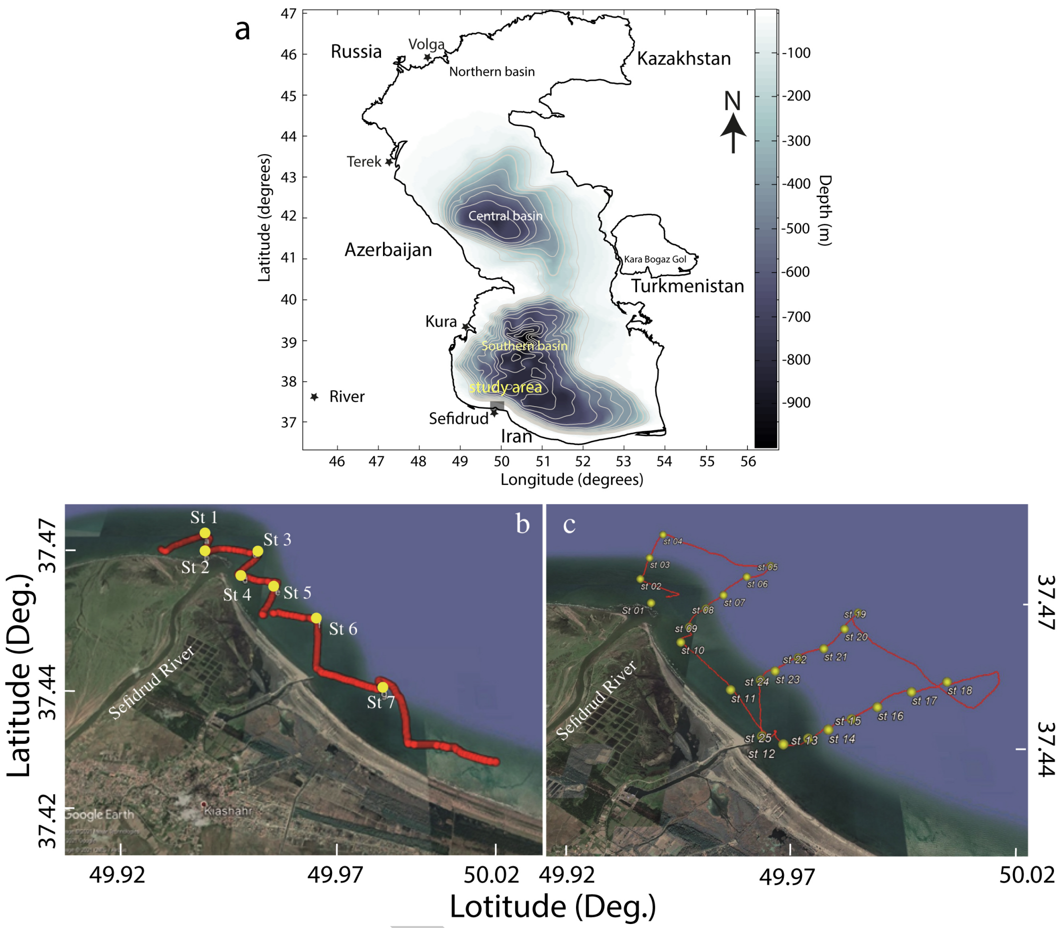

Figure 1. Caspian Sea and study area, a) whole Caspian Basin with main rRivers b) first deployment (13 February 2021), and c) second deployment (21 November 2021) paths and stations.

edge gap in local nearshore hydrodynamic processes. It is noteworthy that previous studies have predominantly addressed the general circulation and hydrodynamics of the CS in the offshore and large-scale studies in terms of field measurements and numerical modelling (Azizpour and Ghaffari, 2023; Komijani et al., 2019; Masoud et al., 2019), with only a limited number of studies focused on continental shelf (Ghaffari and Chegini, 2010; Sabet and Barani, 2011). Moreover, some issues in studying the current field effects of contaminants in the southern nearshore areas remain unresolved.

The use of satellite imagery and remote sensing data enables the identification of large and mesoscale features in marine environments, such as surface currents, hydrographic properties, sea level anomalies, and wave dynamics (Andi et al., 2021; Azizpour and Ghaffari, 2023; Kouraev et al., 2011). Remote sensing data have inherent limitations in coastal waters, primarily due to insufficient spatial resolution for nearshore processes (Teodoro, 2016). Satellite monitoring is further hindered by persistent cloud cover along the Caspian coast, which often obscures the sea surface and prevents reliable observation of nearshore phenomena (Gilmet, 2022). Consequently, direct field measurements are indispensable for obtaining reliable hydrodynamic data in the complex nearshore zone (Azizpour et al., 2016).

River nutrients and other substances are partly trapped in the coastal zone or exchanged with offshore areas through horizontal advection and mixing (Väli et al., 2024). The exchange of these substances and nutrients is facilitated by eddies, river plumes, or wind, and has been reported in several cases, such as in the Baltic Sea (Laanemets et al., 2009; Lass et al., 2010), southwestern European rivers (Romero et al., 2013), and the Gulf of Mexico (Mason et al., 2016). The role of coastal currents and sub-mesoscale eddies in nutrient and pollutant transport and retention has been

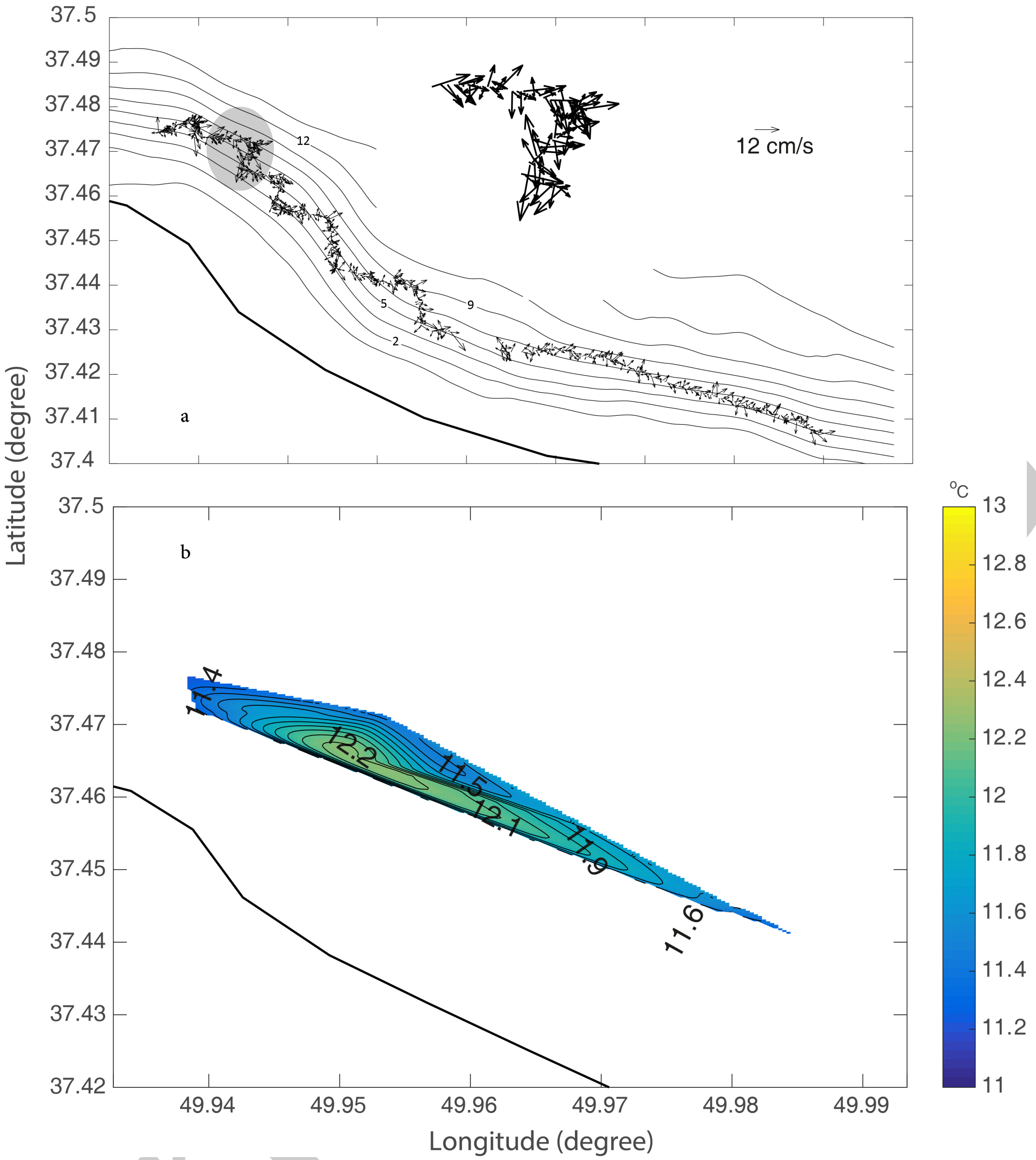

Figure 2. Field measurements of the first deployment for a) ADCP current data at surface (red) and near bednear-bed layer (black), and b) CTD (water temperature).

examined in several studies (e.g., Kubryakov et al., 2023). In their study of the Black Sea, the authors used high- and medium-resolution satellite imagery and a NEMO model to reveal that cyclonic eddies are key mechanisms for trapping and transporting coastal waters.

Understanding coastal hydrodynamics is critical for identifying the distribution of pollutants in nearshore areas. This study investigates the impacts of sub-mesoscale eddies on the trapping and dispersal of contaminants, specifically within the coastal region of the Sefidrud River. We assume that the type of eddy present plays a pivotal role in determining whether pollutants disperse or accumulate. The findings of this research will contribute to a better understanding of the factors governing pollutant distribution, ultimately informing management and mitigation strategies to protect marine ecosystems.

2. Material and methods

2.1 Study area

The study area is located on the southern coast of the CS, east part of Bujagh National Park, off the mouth of the Sefidrud River (Figure 1). The Anzali Lagoon is located to the west of the study area. This coastal region, extending to a depth of 15 m, is bounded by longitudes 49.90°to 50.12°E and latitudes 37.39°to 37.53°N. The Sefidrud River, the greatest river on the Iranian coast of the CS with an average discharge of ∼ 50 m^3/s (www.glrw.ir/?l=EN), originates

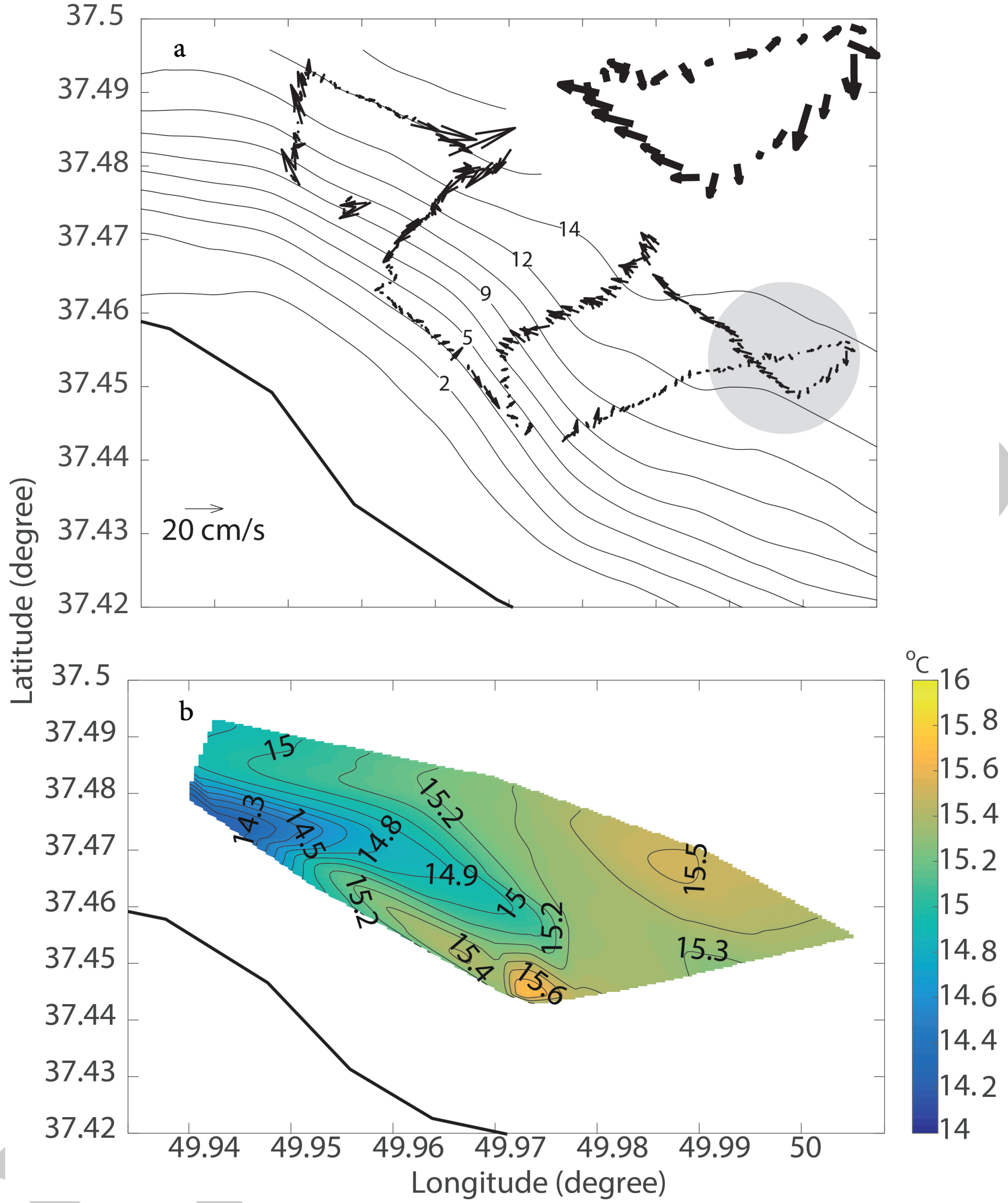

Figure 3. Field measurements of the second deployment for a) ADCP current data at surface (red) and near bednear-bed layer (black), and b) CTD (water temperature).

from the Zagros and Alborz mountain ranges (Beni et al., 2013). It is a primary conduit for land-based pollutions into the southern CS (Costantini et al., 2021).

2.2 Field measurements

Field measurements consist of measuring water current speed and direction using a vessel-mounted ADCP (Workhorse Sentinel), profiles of physical oceanographic parameters using CTD, and collecting water samples using Niskin bottle. For dissolved nutrient analysis, the water samples were immediately filtered on board through 0.45 µm cellulose acetate syringe filters. The filtrate was collected in high-density polyethylene bottles and preserved in near freezing temperature until laboratory analysis (Grasshoff et al., 1999). The time between water sampling and laboratory analysis was less than 12 hours. Field measurements were conducted during two seasons, with the first deployment on 13 February and the second on 21 November 2021. The surveyed water depth ranged from 2.5 to 15 m. A vessel-mounted 600 kHz Teledyne RDI Workhorse Broadband ADCP, interfaced with a Garmin GPSMAP 521s and a laptop computer, was used to obtain detailed current profiles.

Table 1. Quantity of nutrients in the stations of the first deployment.

No.	Station	Position		PO4(ppb)	NO3 (ppb)
		Longitude (deg.)	Latitude (deg.)		
1	St 01	49.938880	37.471985	9.05	125.63
2	St 02	49.949704	37.466161	11.77	115.63
3	St 03	49.958284	37.463059	9.72	59.38
4	St 04	49.969426	37.455137	6.09	35.00
5	St 05	49.984457	37.440320	5.64	39.38

Table 2. Quantity of nutrient in the stations of second deployment.

No.	Station	Position		PO4(ppb)	NO3 (ppb)
		Longitude (deg.)	Latitude (deg.)		
1	St 01	37.47393	49.94382	7.00	51.88
2	St 05	37.4828	49.96963	8.36	70.00
3	St 07	37.47387	49.96025	14.73	73.75
4	St 09	37.46608	49.95448	15.73	85.63
5	St 11	37.45187	49.96597	10.41	116.25
6	St 12	37.4426	49.97393	15.64	130.63
7	St 15	37.44658	49.9863	9.27	101.88
8	St 18	37.45455	50.00512	24.95	125.63
9	St 19	37.46982	49.99038	16.32	120.63
10	St 21	37.46152	49.98173	11.32	122.50
11	St 23	37.45733	49.97325	12.00	110.63

The ADCP was installed in a downward-looking position on the starboard side of a small boat (~ 4 min length), with its transducer approximately 80 cm bellow water surface. All instruments were calibrated according to established methods prior to the field measurements (Joyce, 1989; Khosravi et al., 2018). The ADCP was equipped with bottom-track firmware, an internal compass, and tilt sensors. During deployments, the vessel's velocity was up to 2.5 m/s. The vessel-mounted ADCP survey provides a direct and accurate estimate of the water dynamics, both spatially and temporally. Velocity profiles were averaged over ensembles for 60-second intervals (representing ~ 100 m). For this study, we used the averaged velocity for the surface and near-bed layers. In shallower areas, surface layer data were used instead of near-bed data. Temperature and salinity profiles were measured at several stations using an Ocean Seven 316 CTD (Figure 1, yellow dots) during both deployments. Water sampling was conducted at a subset of these stations (seeTables 1 and 2). To assess phosphates and nitrate concentrations, subsurface water samples were collected in triplicate, and the mean value was used in subsequent analysis. The water samples were immediately filtered on-site through 0.45 µm syringe filters, frozen at −80°C, and subsequently transferred to the laboratory for analysis. The field measurement data underwent a two-stage quality control procedure involving spike removal via visual inspection and the flagging of outliers exceeding two standard deviations. Small gaps in the records were filled using linear interpolation between adjacent values (Azizpour and Ghaffari, 2023; Garcia, 2010).

2.3 Laboratory procedures

The transferred water samples were treated to determine the concentrations of dissolved inorganic nutrients according to the Grasshoff method (Grasshoff, 1983), using a UV-Vis spectrophotometer (Analytic Jena, Specord 210 model) at the Iranian National Institute for Oceanography and Atmospheric Science laboratory. The Colorimetric method was employed to analyze the nutrients, and light absorbance was measured following the standard procedures outlined in MOOPAM (Environment, 1999; Manbohi and Gholamipour, 2020). Phosphates (PO_4^{-3}) concentrations were measured at a wavelength of 882 nm using the molybdate blue method (Murphy and Riley, 1962). Briefly, ammonium molybdate and antimony potassium tartrate were added to each sample. The resulting complex was reduced to a blue complex by the addition of ascorbic acid, and its absorbance was measured. Nitrate (NO_3^-) concentrations were measured by passing the samples through a copper-coated cadmium reduction column to reduce nitrate to nitrite. The resulting nitrite was determined colorimetrically at 540 nm, based on its reaction with an aromatic amine. The measured absorbance is proportional to the combined concentration of nitrate and nitrite. Finally, nitrate concentration was obtained by subtracting any nitrite values in the sample (Wood et al., 1967).

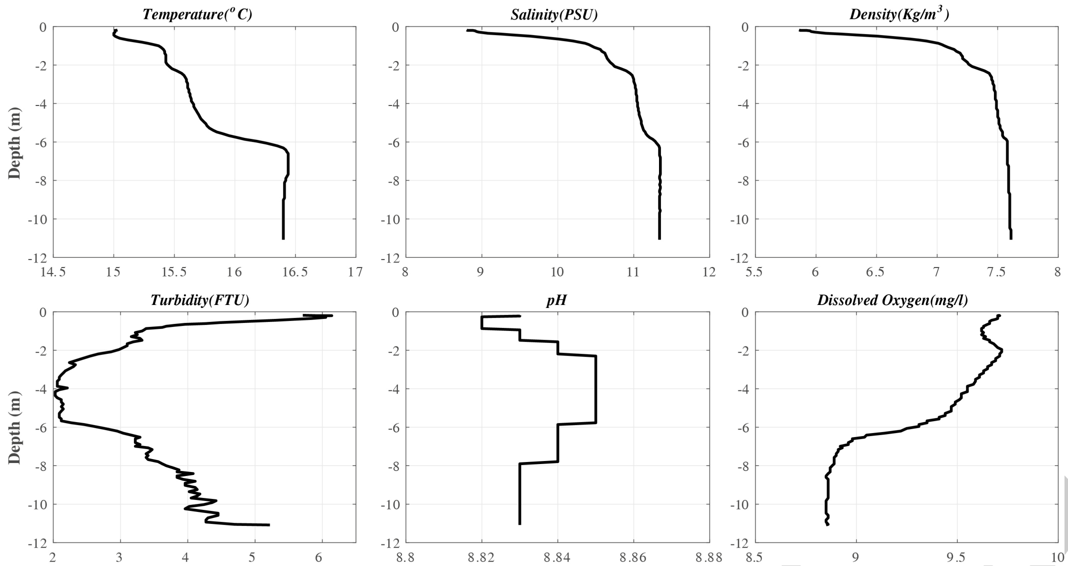

Figure 4. Profiles of physicochemical parameters at station 18 are recorded by CTD around the core of sub mesoscale eddy.

Figure 5. A picture of contaminants and foam about a sub-mesoscale eddy that formed around station 18 (see Figure 1c for the position of the station).

3. Results and discussion

3.1 Hydrodynamics results

The results of the ADCP and CTD measurements for both deployments are presented in Figures 2 and 3. Figure 2a shows current velocity at the surface and near-bed layers for the first deployment, which was conducted along zigzag transects. The maximum speed of the current exceeds 35 cm/s. While the direction of current along the Iranian Coast of the CS is eastward (Zaker et al., 2011), local current direction changes owing to the influence of wind (Ghaffari and Chegini, 2010), and more notably, by

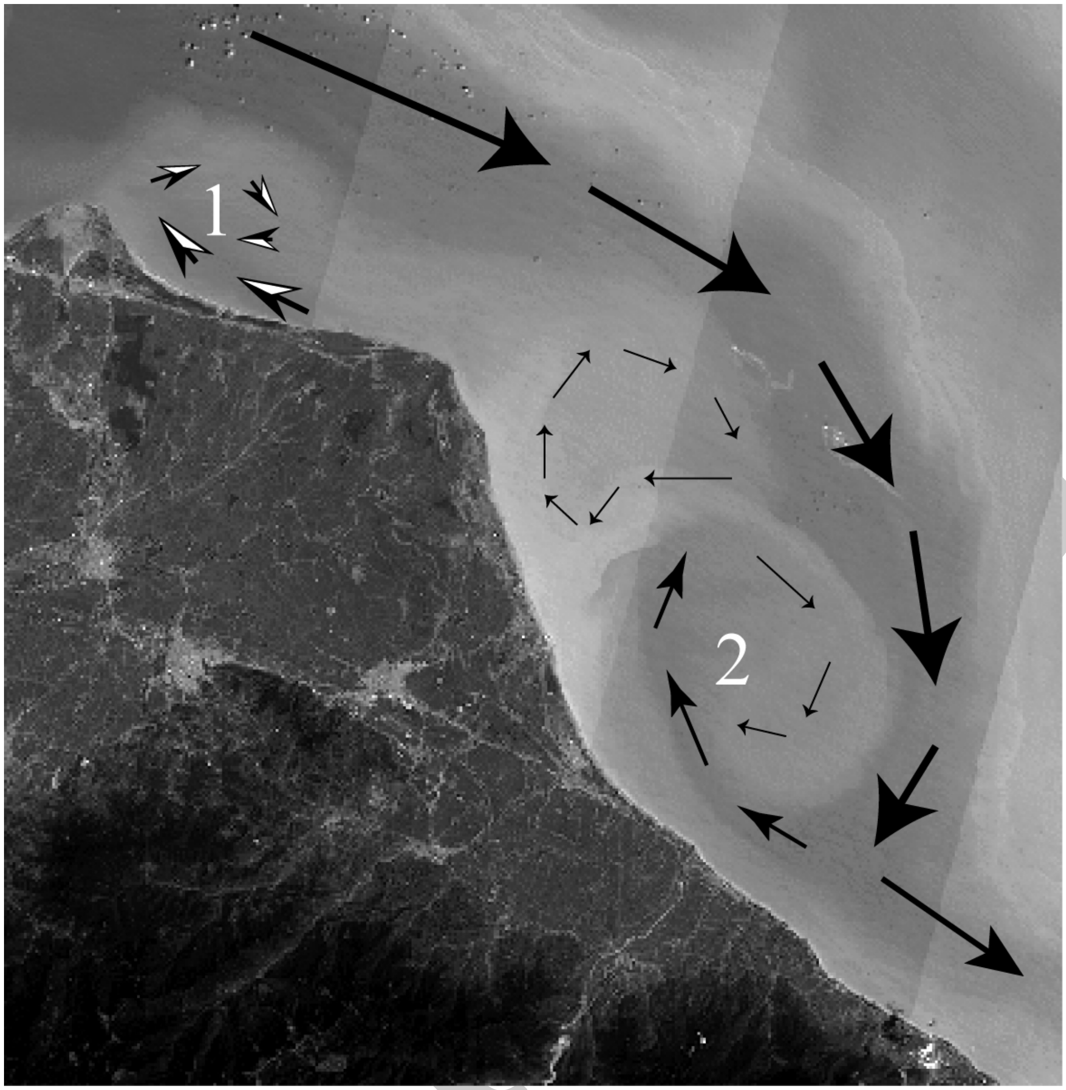

Figure 6. Image of Sentinel 2 mission around study area in the southern Caspian Sea (2021.July, July 04 7:26'). The arrows indicate that eddies form near the shore and originate from the main CS current.

the changes of coastal geometry (Beni et al., 2013), suggesting the presence of water rotation and the formation of coastal eddies. Observations and field research of local fishermen partially confirm the claim. Weather conditions were stable during the field measurements, with wind speed exceed up to ~ 4 m/s.

A warm core sub-mesoscale eddy was identified directly in front of the Sefidrud River mouth, as evidenced by the water temperature contours in Figure 2b. The water temperature contours show an anticyclonic sub-mesoscale eddy in the area. Anticyclonic warm core eddies (in the Northern Hemisphere) are characterized by clockwise rotation and an interior downwelling flow, linking convergent surface waters with divergent flows at depth. According to Figure 2b, the temperature difference between the eddy's core and the surrounding water was about 0.8 °C. Due to the spatial limitations of the current data, the full structure of the sub-mesoscale eddy was not completely detected; however, its signature was partially detectable. No significant difference in the current speed and direction was observed between the surface and near-bed layers, except in the immediate vicinity of the sub-mesoscale eddy (around 37.46°N). The formation of this sub-mesoscale eddy is likely attributed to the horizontal temperature gradient created by the inflow of the Sefidrud River. Furthermore, the vertical temperature and salinity profiles indicate that the eddy structure extended from the surface to the bottom.

Figure 3 shows current vectors and surface water temperature for the second deployment. With getting distance from the coast to the deepest stations, the current speed was increased. An obvious clockwise sub-mesoscale eddy was identified around station 18 (Figure 3a). This eddy was extended from the surface to the near-bed, with a substantial difference in current speed between these two layers. During the second deployment, at least two sub-mesoscale eddies were observed, formed on two sides of the river plume (Figure 3b). A possible explanation for this is that the river plume bifurcates eddies along its sides. This process was observed during a period of exceptional meteorological calm, with a maximum wind speed of ~ 2 m/s. Around the 18th station, the sub-mesoscale eddy is expanded from surface to near bed, with current speeds showing a pronounced vertical gradient, decaying from the surface to the seabed.

High-speed winds cause the eddies to dissipate in the nearshore. Wind-generated currents change current speed and direction at the nearshore (Beni et al., 2013) and consequently change the eddy's structure. As the eddy kinetic energy decreases, the eddy dissipates. In the nearshore region, coastal currents and waves transport contaminants toward the beach. Depth average current speed around sub-mesoscale eddy was about 10 cm/s, where a large amount of contaminants, bubbles, and foam had accumulated (Figure 5). This suggests the eddy created a convergence zone, effectively trapping and concentrating these materials. Station 18 was located near the core of the sub-mesoscale eddy. The sub-surface current speed around this station was about 2–5 cm/s and water hydrodynamics conditions were described as calm. Generally, the current speed was higher during the second deployment, and an increase in river plume influence on coastal alongshore currents in late winter. Figure 4 shows profiles of physicochemical parameters at the 18th station that were recorded by the CTD. Temperature, salinity, and density staircases observed between 2 and 6 m depth were revealed the influence of the eddy on the water column's vertical structure. Minimum and maximum values of turbidity and pH were observed at about 6 m depth, within the lower part of the eddy. This distribution is likely caused by the downwelling effect of an anticyclonic eddy generated in the area, which transports surface water to lower depths. Furthermore, while the maximum dissolved oxygen concentration was observed in the surface layer during the cold season, the subsurface eddy acted to transfer this oxygen-rich water to lower depths. Similar to the first survey, a warm sub-mesoscale core was observed in the area (Figure 3b). The Sefidrud River plume appears to have been responsible for the formation of several eddies. The surface temperature of the river plume was about 13.0°C, contrasting with the surrounding water temperature of about 15.3°C. The temperature of the eddy's core was about 15.3°C. The presence of this warm core is a key indicator of anticyclonic eddies. Warm core eddy causes convergence of nutrients derived from the river plume, as well as marine contaminants, in the core of the eddy (Figure 5). Therefore, higher concentrations of nutrients are expected around the eddy's core.

3.2 Water chemistry results

The nutrient analysis of the water samples (Table 1) reveals that the highest concentrations were observed at the mouth of the Sefidrud River, identifying it as the main nutrient source. From west to east, the quantities of nutrients were decreased, a pattern attributed to a sub-mesoscale anticyclonic eddy. This eddy drives a downwelling process that transports surface nutrients to the lower layer of the water column. The nutrient concentration was remarkable around the eddy's core (station 03).

Table 2 shows the data on phosphate and nitrate in the water samples in some selected stations. Generally, the values increase from west to east of the study area, reflecting the dispersal of the Sefidrud River plume. The lowest values of nutrients were recorded in the westernmost stations, while the maximum amount was recorded around the station 18, which was located near the eddy's core. The results of two surveshow that nearshore sub-mesoscale eddies contribute to the accumulation of contaminants in the region in front of the Sefidrud River. Recently, Manbohi et al. (2021) reported that microplastic pollution levels off the Sefidrud River showed an increasing trend from inshore to offshore, unlike other regions in the South Caspian influenced by river plume. It seems that nearshore sub-mesoscale eddies in this area transport pollution into deeper waters. Consequently, mapping the potential zones for eddy formation would facilitate the targeted collection of accumulated nearshore contaminants. This strategy presents a low-cost opportunity for mitigating damage to the marine environment.

3.3 Eddy generation mechanism

In a rotating fluid, sub-mesoscale eddies can be generated through several mechanisms: (1) the interaction of flows with barriers, such as an offshore main current and geomorphological features like islands or headlands; (2) the convergence of two flows in opposite directions; and (3) barotropic and baroclinic instabilities (Raeisi et al., 2020). A Sentinel-2 satellite image from 4 July 2021, covering the study area, is shown in Figure 6. It seems that the primary reason for sub-mesoscale eddy generation in this area appears to be geomorphological, involving the cape at the Sefidrud River mouth (Figure 6, area 1), as well as the dissipation of kinetic energy (KE) from the main current (bold arrows) as it approaches the coastline (Figure 6, area 2). This latter mechanism points to eddy generation through horizontal shear instability.

When the main currents of the CS approach the nearshore, bed friction disrupts the pressure balance across the current, or jet. This loss of pressure balance triggers a shear instability, which causes the current to meander along the shoreline and generates eddies in the shallower area (Ji et al., 2018). The instability caused by the horizontal velocity shear extracts energy from the mean flow.

4. Conclusion

Nearshore sub-mesoscale eddies are important phenomena that play vital role in the transport of heat, nutrients, and marine pollutions in coastal areas. Due to their limited spatial and temporal scales, small and meso-scale eddies are typically undetectable in satellite imagery, making direct field measurements the most reliable method for their identification and study in the coastal waters, although satellite images greatly helps in finding the boundaries of this phenomenon. On the other hand, identifying areas where contaminants are likely to accumulate is also valuable for marine environmental protection. However, field measurements have inherent limitations. These include unfavorable weather conditions and the inability to capture sub-mesoscale eddies with adequate temporal and spatial resolution.

In this paper, we used field measurements data to detect potential formation areas of coastal sub-mesoscale eddies. Due to geomorphological and geometry features and shear instability of the horizontal velocity, formation of sub-mesoscale eddies were possible (Figure 6), even though they were disappeared during stormy conditions. Stormy conditions cause to generate high amplitude waves at near shore of the CS that lead to intense vertical mixing, creating a homogeneous water column from surface to the bed. On the other hand, sub-mesoscale eddies were expanded from surface to the bed, consequently, the storm-induced reduction in kinetic energy caused them to dissipate.

Due to the eastward direction of the main current of the southern CS (Azizpour and Ghaffari, 2023; Dyakonov and Ibrayev, 2020; Ghaffari and Chegini, 2010), the identified eddies are predominantly anticyclonic. These types of eddies are convergent, accumulating marine pollutants and nutrients. The main source of nutrients in the study area is riverine. When these nutrient-rich waters enter the coastal zone, they are effectively trapped by sub-mesoscale eddies. The convergent surface flow that characterizes these eddies accumulates nutrients, and the associated collapse in the eddy core facilitates their downward transport. This mechanism effectively redistributes the coastal nutrient load offshore.

Bakhtiari et al. (2024) explored sub-mesoscale eddies off the Sefidrud River and Rudsar regions using numerical modeling and MODIS images from 2010 to 2014. Their results showed distinct turbid current patterns and sub-mesoscale eddies generated by the Sefidrud River cape and prevailing winds. The sub-mesoscale eddies were influenced by the discharge from the Sefidrud River. Depending on the current direction, the types of eddies are predictable; for example, easterly currents generate anticyclonic eddies and vice versa. The radius of sub-mesoscale eddies in the area was less than 20 km, and most of them were anticyclonic.

Generated eddies in the wintertime are obviously due to an increase in current velocity. Sefidrud River cape deflects the current direction, especially when the current speed increases. Under calm weather conditions, several sub-mesoscale eddies were generated in the study area. The core of these eddies exhibited higher temperature and salinity than the surrounding waters. Warm core eddies cause downwelling in the ocean, and nutrient-poor waters as well as low biomasses may converge and be downwelled (Azizpour et al., 2021; Raeisi et al., 2020). This convergence leads to elevated concentrations of contaminants and nutrients within the eddy core.

A comprehensive assessment of the impact of sub-mesoscale eddies on coastal pollutant transport requires future studies with expanded spatial coverage and seasonal resolution.

Conflict of interest

None declared.

References

Aladin, N., Plotnikov, I., 2004. *The Caspian Sea*. Lake Basin Manage. Initiative Thematic Paper.

Andi, S., Rashidi Ebrahim Hesari, A., Farjami, H., 2021. *Detection of internal waves in the Persian Gulf*. Remote Sens. Lett. 12, 190–198.

Azizpour, J., Farjami, H., Ghaffari, P., 2021. *Intrathermocline eddies in the Strait of Hormuz*. Arabian J. Geosci. 14, 2118.

Azizpour, J., Ghaffari, P., 2023. *Low-frequency sea level changes in the Caspian Sea: long-term and seasonal trends*. Climate Dynam. 1–11.

Azizpour, J., Siadatmousavi, S.M., Chegini, V., 2016. *Measurement of tidal and residual currents in the Strait of Hormuz*. Estuar. Coast. Shelf Sci. 178, 101–109.

Bakhtiari, A., Shad, E., Siadatmousavi, S.M., 2024. *Exploring submesoscale eddies in the southern Caspian Sea: A focus on rudsar Rudsar and Sefidrud regions*. Deep Sea Res. Pt. I: Oceanograph.Res. Papers 208, p. 104316.

Beni, A.N., Lahijani, H., Harami, R.M., Leroy, S., Shah-Hosseini, M., Kabiri, K., Tavakoli, V., 2013. *Development of spit–lagoon complexes in response to Little Ice Age rapid sea-level changes in the central Guilan coast, South Caspian Sea, Iran*. Geomorphology 187, 11–26.

CEP, 1998. *National Report, Russian Federation*. Caspian Environment Programme, Baku, Azerbaijan.

CEP, 2011. *Caspian Sea State of the Environment*, 102 pp.

Costantini, M.L., Agah, H., Fiorentino, F., Irandoost, F., Trujillo, F.J.L., Careddu, G., Calizza, E., Rossi, L., 2021. *Nitrogen and metal pollution in the southern Caspian Sea: a multiple approach to bioassessment*. Environ. Sci. Pollut.Res.28, 9898–9912.

Dyakonov, G.S., Ibrayev, R.A., 2020. *High-resolution data on mesoscale dynamics of the Caspian Sea upper layer,* *obtained in a numerical reconstruction*. Data In Brief 30, 105368.

Ehteshami, M., Dravishi, G., ShirAli, E., 2017. *Caspian Sea, Leading Threats in terms of Pollution and Hydrological Crises*.

Environment, R.O.f.t.P.o.t.M., 1999. *Manual of oceanographic observations and pollutant analyses methods (MOOPAM)*, 3rd edn., Kuwait.

Garcia, D., 2010. *Robust smoothing of gridded data in one and or higher dimensions with missing values*. Computat. Statistics Data Anal. 54, 1167–1178.

Ghaffari, P., Chegini, V., 2010. *Acoustic Doppler Current Profiler observations in the southern Caspian Sea: shelf currents and flow field off Feridoonkenar Bay, Iran*. Ocean Sci. 6, 737–748.

Ghaffari, P., Lahijani, H., Azizpour, J., 2010. *Snapshot observation of the physical structure and stratification in deep-water of the South Caspian Sea (western part)*. Ocean Sci. 6, 877–885.

Gilmet, 2022. https://gilmet.ir/.

Grasshoff, K., Kremling, K., Ehrhardt, M., 1999. *Methods of seawater analysis*, Chapter 10 – *Nutrients. Methods of seawater analysis*, 159–228.

Ji, J., Dong, C., Zhang, B., Liu, Y., Zou, B., King, G.P., Xu, G., Chen, D., 2018. *Oceanic eddy characteristics and generation mechanisms in the Kuroshio Extension region*. J. Geophys. Res.-Oceans 123, 8548–8567.

Joyce, T.M., 1989. *On in situ "calibration" of shipboard ADCPs*. J. Atmos. Oceanic Tech. 6, 169–172.

Khosravi, M., Siadatmousavi, S.M., Vennell, R., Chegini, V., 2018. *The transverse dynamics of flow in a tidal channel within a greater strait*. Ocean Dynami. 68(2), 239–254.

Komijani, F., Chegini, V., Siadatmousavi, S., 2019. *Seasonal variability of circulation and air-sea interaction in the Caspian Sea based on a high resolution circulation model*. J. Great Lakes Res. 45, 1113–1129.

Kouraev, A., Crétaux, J.-F., Lebedev, S., Kostianoy, A., Ginzburg, A., Sheremet, N., Mamedov, R., Zakharova, E., Roblou, L., Lyard, F., 2011. *Satellite altimetry applications in the Caspian Sea*, Coastal Altimetry Springer, 331–366.

Kubryakov, A., Aleskerova, A., Plotnikov, E., Mizyuk, A., Medvedeva, A., Stanichny, S., 2023. *Accumulation and cross-shelf transport of coastal waters by submesoscale cyclones in the Black Sea*. Remote Sens. 15(18), p. 4386.

Laanemets, J., Zhurbas, V., Elken, J., Vahtera, E., 2009. *Dependence of upwelling-mediated nutrient transport on wind forcing, bottom topography and stratification in the Gulf of Finland: model experiments*. Boreal Environ. Res. 14(1), p. 213.

Lass, H.U., Mohrholz, V., Nausch, G., Siegel, H., 2010. *On phosphate pumping into the surface layer of the eastern Gotland Basin by upwelling*. J. Marine Syst. 80(1–2), 71–89.

Manbohi, A. and Gholamipour, S., 2020. *Utilizing chemometrics and geographical information systems to evaluate spatial and temporal variations of coastal water quality*. Reg. Stud. Marine Sci. 34, p.101077.

Manbohi, A., Mehdinia, A., Rahnama, R., Dehbandi, R., 2021. *Microplastic pollution in inshore and offshore surface waters of the southern Caspian Sea*. Chemosphere 281, 130896.

Mason, O.U., Canter, E.J., Gillies, L.E., Paisie, T.K., Roberts, B.J., 2016. *Mississippi river plume enriches microbial diversity in the northern Gulf of Mexico*. Frontiers Microbiol. 7, p. 1048.

Masoud, M., Pawlowicz, R., Namin, M.M., 2019. *Low frequency variations in currents on the southern continental shelf of the Caspian Sea*. Dynam. Atmos. Oceans 87, 101095.

Murphy, J., Riley, J.P., 1962. *A modified single solution method for the determination of phosphate in natural waters*. Anal. Chim. Acta 27, 31–36.

Raeisi, A., Bidokhti, A., Nazemosadat, S.M.J., Lari, K., 2020. *Mesoscale eddies and their dispersive environmental impacts in the Persian Gulf*. Chinese Phys. B 29, 084701.

Romero, E., Garnier, J., Lassaletta, L., Billen, G., Le Gendre, R., Riou, P., Cugier, P., 2013. *Large-scale patterns of river inputs in southwestern Europe: seasonal and interannual variations and potential eutrophication effects at the coastal zone*. Biogeochemistry 113, 481–505.

Roshan, G., Moghbel, M., Grab, S., 2012. *Modeling Caspian Sea water level oscillations under different scenarios of increasing atmospheric carbon dioxide concentrations*. Iranian J. Environ. Health Sci. Eng. 9, 24.

Sabet, B.S., Barani, G.A., 2011. *Field investigation of rip currents along the southern coast of the Caspian Sea*. Scientia Iranica 18, 878–884.

Safaian, N., Shokri, M., Jabbarian, B., 2004. *Environmental Impact Assessment of Development in the Southern Coast of the Caspian Sea (Northern Iran)*. Polish J. Environ. Stud. 13.

Saleh, A., Hamzehpour, A., Mehdinia, A., Bastami, K.D., Mazaheri, S., 2018. *Hydrochemistry and nutrient distribution in the southern deep-water basin of the Caspian Sea*. Marine Pollut. Bull. 127, 406–411.

Teodoro, A.C., 2016. *Optical satellite remote sensing of the coastal zone environment – An overview*. Environ.Appl. Remote Sens., InTechOpen, London, UK, 165–196.

UNEP, 2006. *Caspian Sea*, (Stolberg, F., Borysova, O., Mitrofanov, I., Barannik, V. and Eghtesadi, P., eds.), GIWA Region. Assess. 23, p. 92.

Väli, G., Meier, H.M., Liblik, T., Radtke, H., Klingbeil, K., Gräwe, U., Lips, U., 2024. *Submesoscale processes in the surface layer of the central Baltic Sea: A high-resolution modelling study*. Oceanologia 66(1), 78–90. https://doi.org/10.1016/j.oceano.2023.11.002

Wood, E.D., Armstrong, F., Richards, F.A., 1967. *Determination of nitrate in sea waterseawater by cadmium-copper reduction to nitrite*. J. Mar. Biol. Assoc. UK 47, 23–31.

Zaker, N., Ghaffari, P., Jamshidi, S., Nouranian, M., 2011. *Currents on the southern continental shelf of the Caspian Sea off Babolsar, Mazandaran, Iran*. J. Coast.Res. 64(SI), 1989–1997. https://www.jstor.org/stable/26482525